Electronic Supplementary Material (ESI) for ChemComm.

Electronic Supplementary Information for

Plasma-enhanced direct splitting of CO_2 to CO over oxygen-deficient Mo-doped CeO_2 catalysts

Li Wang*[a], Xiaomin Du[a], Yanhui Yi[b], Hongyang Wang[a], Masaud Gul[a], Yimin Zhu[a] and Xin Tu*[c]

a. College of Environmental Sciences and Engineering, Dalian Maritime University, Dalian, 116026, P. R. China.

b. State Key Laboratory of Fine Chemicals, School of Chemical Engineering, Dalian University of Technology, Dalian 116012, P. R. China

c. Department of Electrical Engineering and Electronics, University of Liverpool, Liverpool, L69 3GJ, UK.

***Corresponding authors**

liwang@dlmu.edu.cn (Li Wang) and *xin.tu@liverpool.ac.uk* (Xin Tu)

Table of Contents

1. Thermodynamic equilibrium calculation of CO_2 splitting to CO

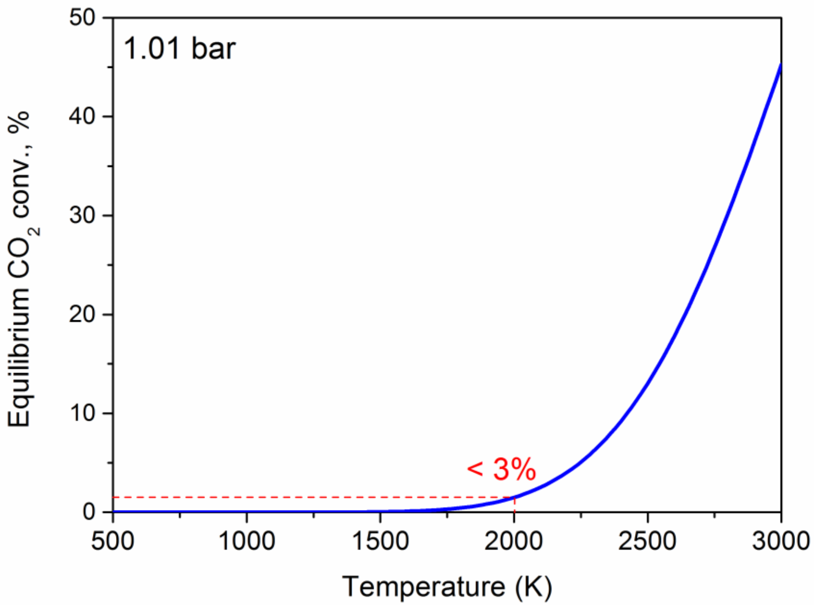

Fig. S1. Thermodynamic equilibrium conversion of CO_2 as a function of reaction temperature

2. Experimental Setup

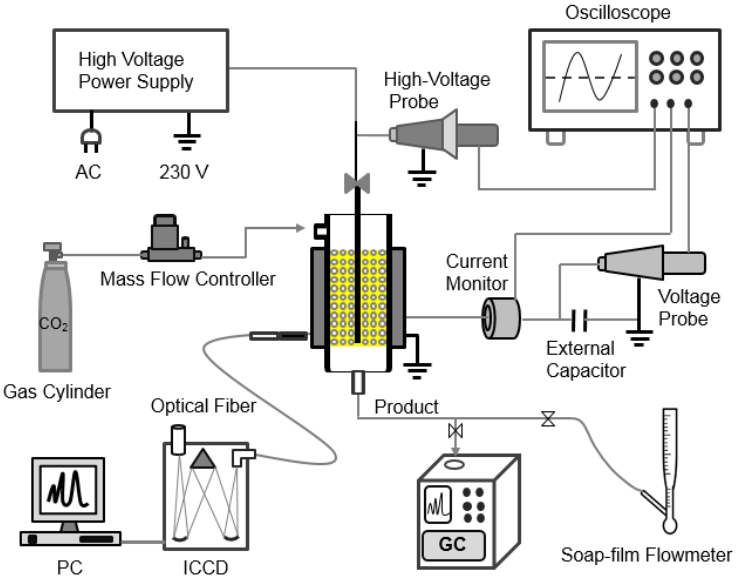

Fig. S2. Schematic diagram of the experimental setup.

CO_2 splitting to CO was carried out in a dielectric barrier discharge (DBD) reactor packed with different catalysts (Fig. S2). The DBD reactor consisted of a pair of coaxial glass cylinders (inner and outer glass tubes). A stainless-steel rod (inner high voltage electrode) with an outer diameter of 2 mm was placed along the axis of the inner glass tube. The discharge length was 20 mm with a discharge gap of 3 mm. The catalyst was packed into the whole discharge area. To understand the effect of reaction temperature on the plasma splitting CO_2, different ground electrodes (circulating water and

Al foil) were used in this study. When using circulating water as a ground electrode, circulating water was filled in the space between the outer surface of the inner glass tube and the inner surface of the outer glass tube, which could effectively remove the heat generated by the discharge and maintain the reaction at around room temperature (~30 ^{o}C). In another case, Al foil instead of circulating water was tightly wrapped outside of the outer glass tube as a ground electrode to maintain the reaction temperature at around 400 ^{o}C. Note no extra heating was used in this study. The gas flow rate of CO_2 was controlled by a mass flow controller with a flow rate of 40 ml/min. The DBD reactor was connected to an AC power supply with a maximum peak voltage of 30 kV and a variable frequency of 7-12 kHz. In this study, the frequency was kept constant at 9 kHz. The electrical signals (applied voltage, current and voltage on an external capacitor) were recorded by a four-channel digital oscilloscope (Tektronix, MDO 3024). The discharge power was calculated using the Lissajous method. A homemade control system was used for the real-time monitoring the discharge power.

The emission spectra of the DBD plasma using different gas compositions (CO_2, CO_2/Ar, and CO_2/N_2) were recorded using a Princeton Instruments ICCD spectrometer (SP 2758) in the range of 200-1200 nm via an optical fiber, which was placed near the ground electrode of the DBD reactor. A 300 g mm^{-1} grating was used in these measurements. The slit width of the spectrometer was fixed at 20 µm.

The change of the gas volume before and after the reaction was measured using a soap-film flowmeter. The gas products were analyzed using a gas chromatograph (GC, Shimadzu GC-2014) equipped with a thermal conductivity detector (TCD) and a flame ionization detector (FID). No carbon deposition was observed on the catalyst surfaces and the inner surface of the DBD reactor after 2 h reaction. The formation of ozone and NO_x was measured by using an FTIR spectroscopy. To evaluate the reaction performance of plasma CO_2 splitting, the specific energy input (SEI), CO_2 conversion (X_{CO_2}), and energy efficiency (E) are defined as the following:

$$\text{SEI (kJ/L)} = \frac{\text{Discharge power (kW)}}{\text{CO}_2\text{ flow rate (L/h)}} \qquad (1)$$

$$X_{CO_2}\,(\%) = \frac{\text{moles of CO}_2\text{ converted}}{\text{moles of CO}_2\text{ in feed}} \times 100 \qquad (2)$$

$$\text{E (mmol/kJ)} = \frac{\text{CO}_2\text{ converted (mmol/h)}}{\text{Discharge power (kW)}} \qquad (3)$$

$$\text{E}(\%) = \frac{\text{CO}_2\text{ flow rate (mol/s)} \times X_{CO_2}(\%) \times \text{VH(kJ/mol)}}{\text{Discharge power (kW)}} \qquad (4)$$

3. Catalyst preparation

All the catalysts were synthesized by incipient wetness impregnation over CeO_2 (Dalian Luming Nanometer Material Co., Ltd.). The metal precursor solution was prepared by dissolving each metal nitrate salt (17.57 g $Fe(NO_3)_3 \cdot 9H_2O$, 12.75 g $Co(NO_3)_2 \cdot 6H_2O$, 12.65 g $Ni(NO_3)_2 \cdot 6H_2O$, 10.51 g $Cu(NO_3)_2 \cdot 3H_2O$, 15.48 g $Mn(NO_3)_2$ solution, 5.09 g NH_4VO_3, 5.48 g $(NH_4)_2Cr_2O_7$, 7.68 g $(NH_4)_6Mo_7O_{24} \cdot 4H_2O$) in water, which was just sufficient to fill the pores of 12 g CeO_2 support. The support was firstly calcined at 400 ^oC for 5 h to remove the impurities (e.g., adsorbed H_2O) in a muffle furnace, before added to the as-prepared precursor solution, and was stirred until it was thoroughly mixed. The resulting mixture was successively kept at room temperature for 3 h, vacuum freeze-dried overnight at -50 ^oC and then dried in air at 120 ^oC for 5 h. The dried sample was calcined in an Ar DBD plasma at 350 ^oC for 3 h. The metal loading was ca. 15 wt.%.

4. Reaction performance

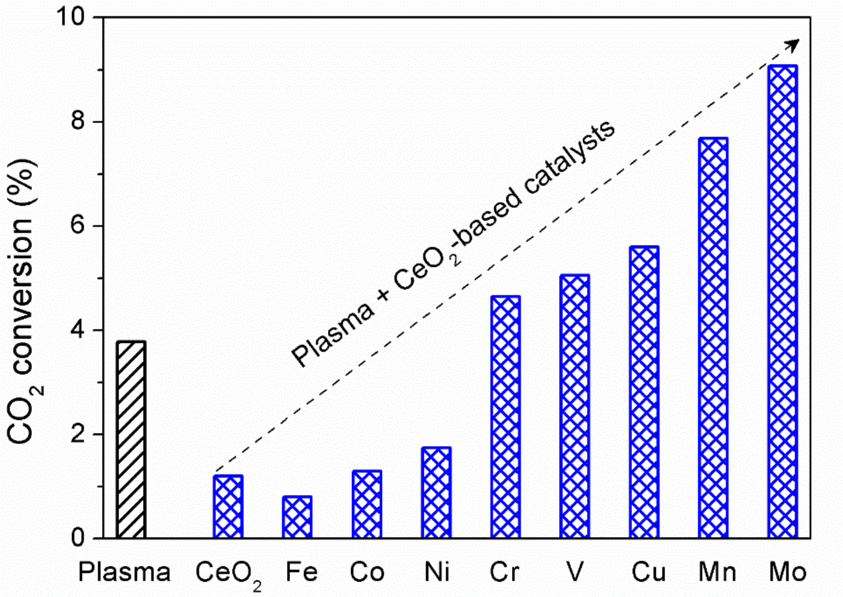

Fig. S3. Influence of different catalysts on plasma-catalytic CO_2 splitting
(CO_2 flow rate 40 ml/min, reaction temperature 400 ^oC, SEI 20 kJ/L, discharge power 13.5 W).

Table S1. A comparison of various catalysts used in plasma-catalytic CO_2 splitting to CO

Catalyst	Plasma type	SEI (kJ/L)	CO_2 conversion (%)	Energy efficiency (%)	Ref
Mo-doped CeO_2	DBD	20	23.2	14.3	This work
$BaTiO_3$	DBD	28	38.3	17.0	[1]
TiO_2	DBD	28	27	12.2	[1]
$Ni/SiO_2 + BaTiO_3$	DBD	132	23.5	3.4	[2]
$Ni/\gamma\text{-}Al_2O_3$	DBD	80	29	4.5	[3]
ZrO_2	DBD	180	38	5.8	[4]
$g\text{-}C_3N_4$	DBD	24	17	8.9	[5]
$FeO_x\text{-}CeO_x/\gamma\text{-}Al_2O_3$	DBD	22.5	28.2	15.7	[6]
NiO/TiO_2	Microwave	30	42	17.2	[7]
Rh/TiO_2	Microwave	-	8	6.0	[8]
TiO_2	Gilding arc	7.2	11	19	[9]

References

[1] D. Mei, X. Zhu, C. Wu, B. Ashford, P. T. William, X. Tu, Appl. Catal. B: Environ. 2016, 182, 525.
[2] K. Zhang, G. Zhang, X. Liu, A. N. Phan, K. Luo, Ind. Eng. Chem. Res. 2017, 56, 3204.
[3] D. Mei, X. Tu, ChemPhysChem 2017, 18, 3253.
[4] K. Van Laer, A. Bogaerts, Energy Technol. 2015, 3, 1038.
[5] N. Lu, D. Sun, C. Zhang, N. Jiang, K. Shang, X. Bao, J. Li, Y. Wu, J. Phys. D: Appl. Phys. 2018, 51, 094001.
[6] B. Ashford, Y. Wang, C. K. Poh, L. Chen, X. Tu, Appl. Catal. B: Environ. 2020,276,119110.
[7] G. Chen, V. Georgieva, T. Godfroid, R. Snyders, M. Delplancke-Ogletree, Appl. Catal. B. Environ. 2016, 190, 115.
[8] L. F. Spencer, A. D. Gallimore, Plasma Sources Sci. Technol. 2013, 22, 015019.
[9] H. Zhang H, L. Li, R. Xu, J. Huang, N. Wang, X. Li, X. Tu, Waste Dispos. Sustain. Energy 2020, 2, 139.

Table S2. Performance of CO_2 splitting to CO under different reaction conditions

Approach	Reaction temperature (^{o}C)	Additive gas	CO_2 conversion (%)	Formation rate of CO (mmol/h)	Energy efficiency of CO_2 conversion (mmol/kJ)
Catalyst only	400	-	0	0	0
Plasma only	400	-	3.8	4.1	0.08
Plasma + CeO_2	400		1.2	1.3	0.03
Plasma + Mo-doped CeO_2	400	-	9.1	9.8	0.20
	30	-	13.5	14.5	0.30
Plasma + Mo-doped CeO_2	30	Ar	20.5	22.0	0.36
		N_2	23.2	24.9	0.41

5. Catalyst characterization

XRD patterns of CeO_2 supported metal catalysts

Fig. S4 showed the XRD patterns of the as-synthesized CeO_2 supported metal catalysts. The pure CeO_2 support exhibited a series of diffraction peaks at 28.45^{o}, 33.01^{o}, 47.34^{o}, 56.25^{o}, 59.04^{o}, 69.36^{o}, 76.67^{o} and 79.00^{o}. These peaks can be indexed to (111), (200), (220), (311), (222), (400), (331) and (420), respectively, which reflects a cubic fluorite structure of ceria phase with a space group Fm3m (JCPDS, 34-0394). In the XRD patterns of the CeO_2 supported catalysts, the characteristic peaks of CeO_2 were still visible, but the intensity of these peaks decreased. In addition, the as-synthesized CeO_2 supported catalysts (Fe, Co, Ni, Cu, Cr, V, Mn and Mo) exhibited weak but visible peaks, corresponding to their parent metal oxides, Fe_2O_3, Co_3O_4, NiO, CuO, Cr_8O_{21}, V_2O_5, MnO_2, and a two-phase mixture of α-MoO_3 and Mo_4O_{11}.

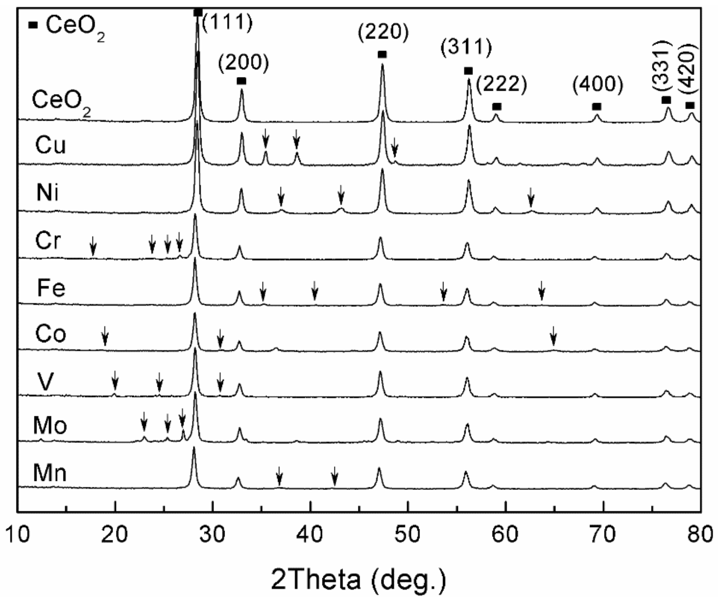

Fig. S4. XRD patterns of pure CeO_2 and as-synthesized catalysts.

TPR analysis of CeO_2 supported metal catalysts

Oxygen vacancy is usually created by the reduction of metal oxide catalysts. Thus, the generation of oxygen vacancy strongly depends on the reducibility of metal oxides. H_2-TPR is extensively used to evaluate the reducibility of metal oxide-based catalysts. Fig. S5 shows the H_2-TPR profiles of as-synthesized catalysts. Clearly, the reducibility of metal oxides strongly depends on the types of metals, and the complete-reduction temperature of the as-synthesized catalysts increased in the order of $Cu/CeO_2 < Ni/CeO_2 < Mn/CeO_2 < Cr/CeO_2 < Mo/CeO_2$. However, the surface-oxygen reduction temperature (i.e., starting-reduction temperature) of these catalysts followed the order of Cu ≈ Mn (ca. 150 °C) < Fe ≈ Co ≈ Ni (ca. 180 °C) < Mo (ca. 310 °C) < V (ca. 440 °C) < Cr (ca. 470 °C)

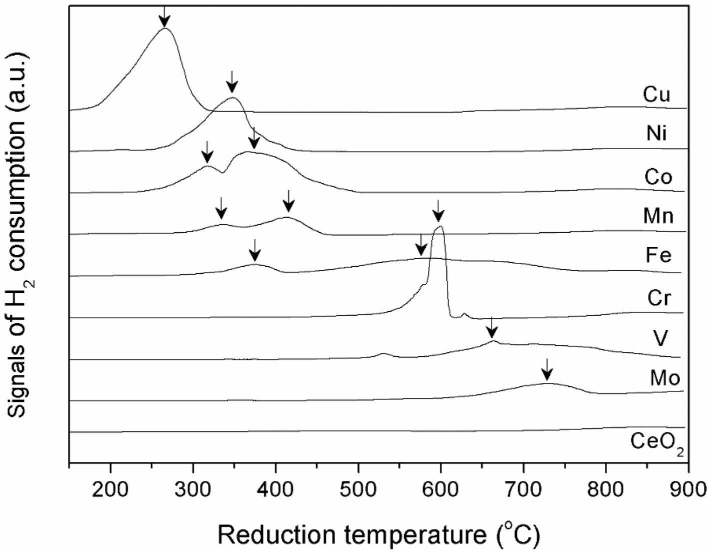

Fig. S5. H_2-TPR profiles of metal-doped CeO_2 catalysts

Calculation of Ce^{3+} and V_O concentration

Peak areas (A) of Ce^{4+} and Ce^{3+} components are normally used to estimate their relative concentration (C) as shown in Fig. S6 (a) and (b). According to the following equations, the concentration of Ce^{3+} in CeO_2 and Mo-doped CeO_2 samples were 30.0% and 40.2%, respectively.

$$A_{Ce^{3+}} = A_{v_o} + A_{u_o} + A_{v'} + A_{u'}$$

$$A_{Ce^{4+}} = A_{v} + A_{u} + A_{v''} + A_{u''} + A_{v'''} + A_{u'''}$$

$$C_{Ce^{3+}} = \frac{A_{Ce^{3+}}}{A_{Ce^{4+}} + A_{Ce^{3+}}} \times 100\%$$

Peak areas (A) of V_O and O_L (lattice oxygen) are used to estimate the relative concentration (C) of V_O, as shown in Fig. S6 (c) and (d). According to the following equation, the relative concentration of V_O in CeO_2 and Mo-doped CeO_2 samples were 21.0% and 30.4%, respectively.

$$C_{V_O} = \frac{A_{V_O}}{A_{V_O} + A_{O_L}} \times 100\%$$

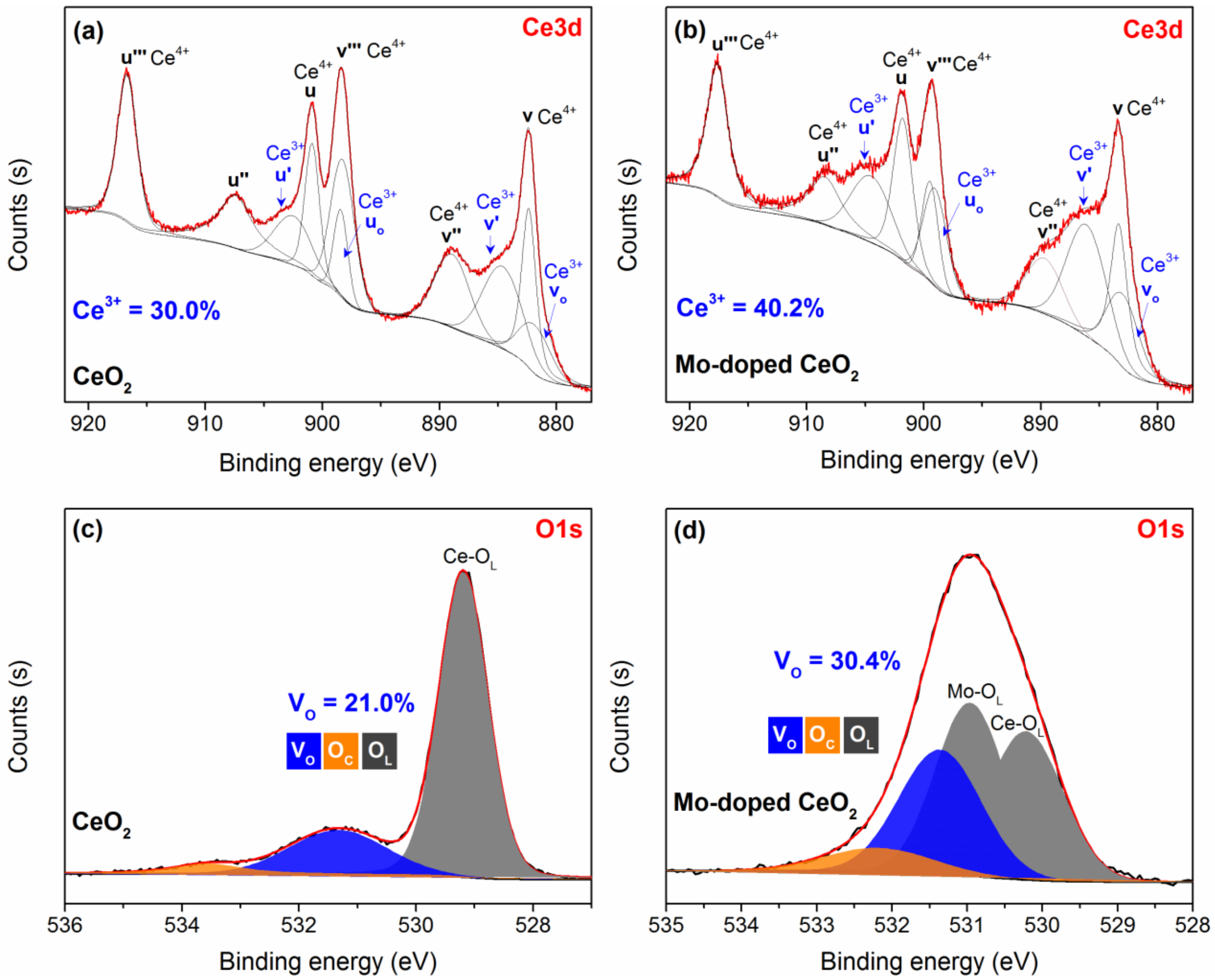

Fig. S6. Deconvoluted XPS spectra of Ce3d and O 1s core levels in CeO_2 and Mo-doped CeO_2 samples.

The binding energies reported in this study were determined using standard C1s peaks at 284.8 eV.

XPS survey spectrum of Mo-doped CeO_2

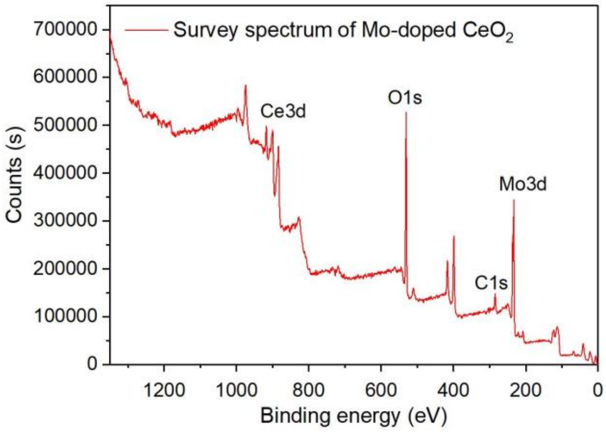

Fig. S7. XPS survey spectrum of Mo-doped CeO_2.

Concentration of Ce^{3+}, Mo^{5+} and V_O

Table S3. Concentration of Ce^{3+}, Mo^{5+} and V_O of the fresh and spent Mo-doped CeO_2 catalysts determined by the corresponding deconvoluted XPS spectra.

Catalyst	Ce^{3+}	Mo^{5+}	V_O
Fresh catalyst	40.2%	11.2%	30.4%
Spent catalyst after reaction at 400 °C	44.7%	12.1%	34.2%
Spent catalyst after reaction at 30 °C with N_2	41.4%	9.2%	31.8%

H_2-TPR profiles of as-prepared Mo-doped CeO_2

H_2-TPR is extensively used to evaluate the metal-support interaction. As shown in Fig. S8, the complete-reduction temperature of Mo/CeO_2 was much higher than that of Mo/γ-Al_2O_3, suggesting the presence of a stronger interaction between Mo and Ce. It might be caused by the decreasing electronegativity of Mo > Al > Ce; thus electrons prefer to transfer from Ce to Mo compared with Al.

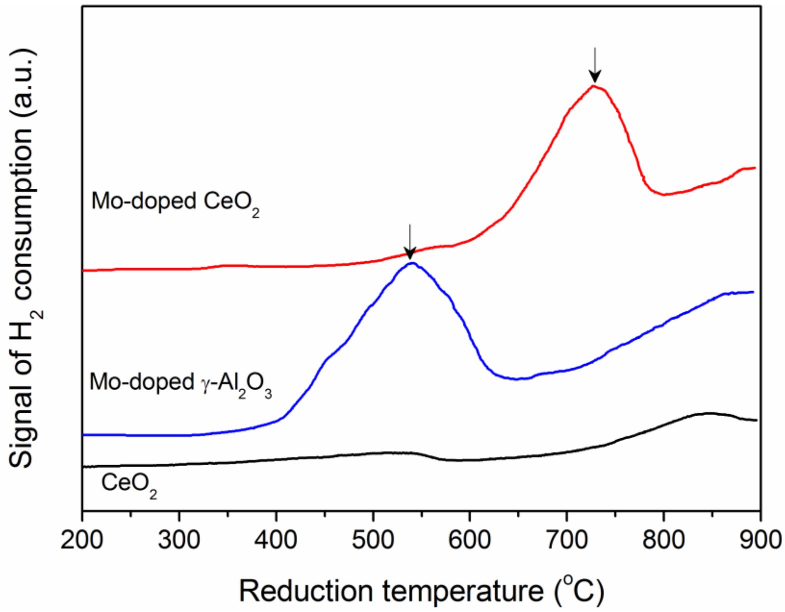

Fig. S8. H_2-TPR profiles of as-prepared Mo/CeO_2, Mo/γ-Al_2O_3 and CeO_2.

SEM/TEM images and BET surface area of Mo-doped CeO_2

SEM images shows that the distribution of CeO_2 nanoparticles was uniform with an average particle size of around 20-30 nm, but the visible agglomeration of nanoparticles was observed as well. In addition, the EDS mapping images exhibit homogeneous distribution of O, Ce and Mo element, and most of these elements existed together, indicating the interaction among Mo, Ce and O.

N_2 physisorption was performed to analyse the specific surface area of CeO_2 and Mo/CeO_2. and The BET surface area of Mo/CeO_2 was only 5.8 m^2/g, much lower than that of CeO_2 (46.5 m^2/g).

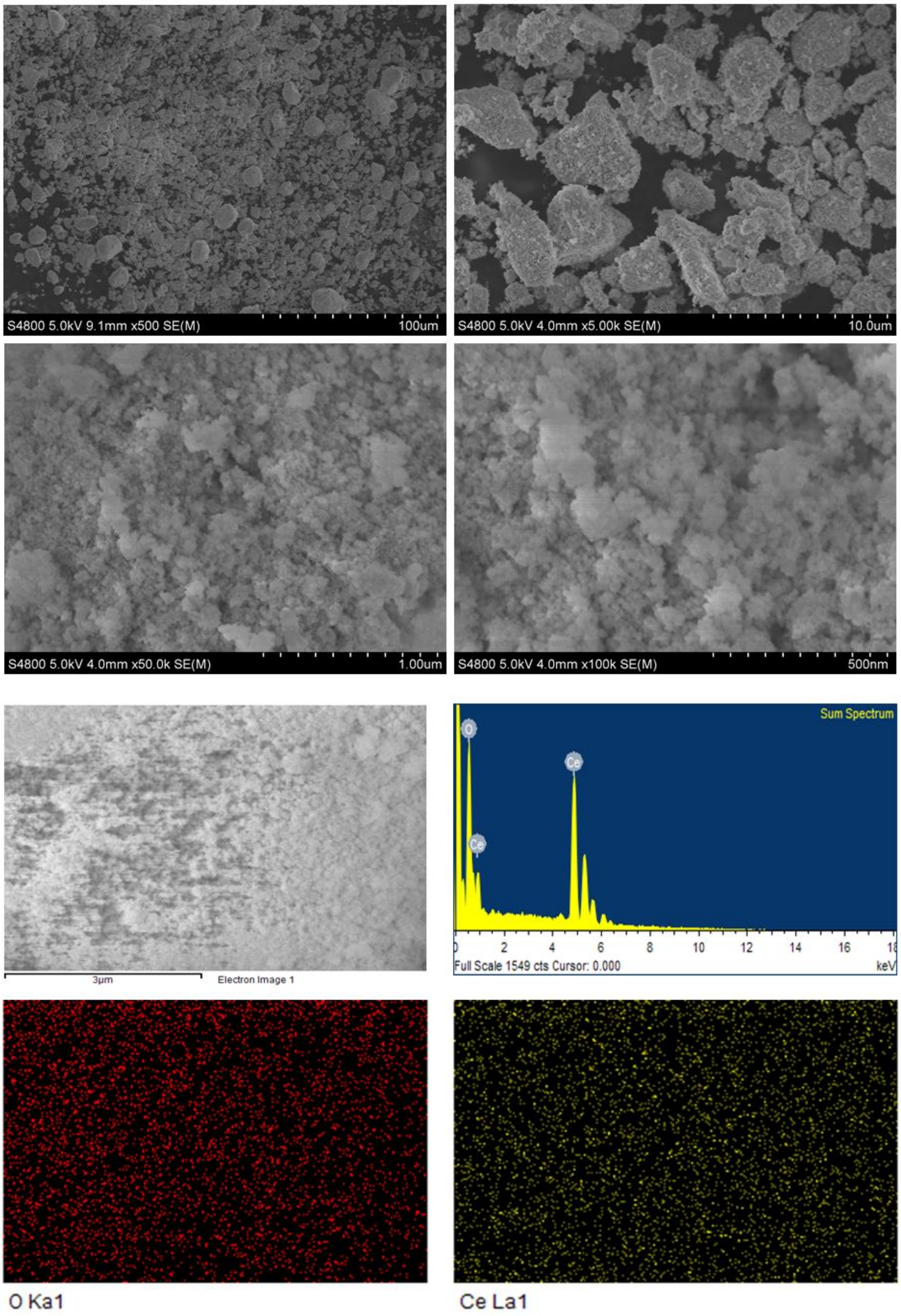

Fig. S9. SEM and SEM-EDS images of CeO_2.

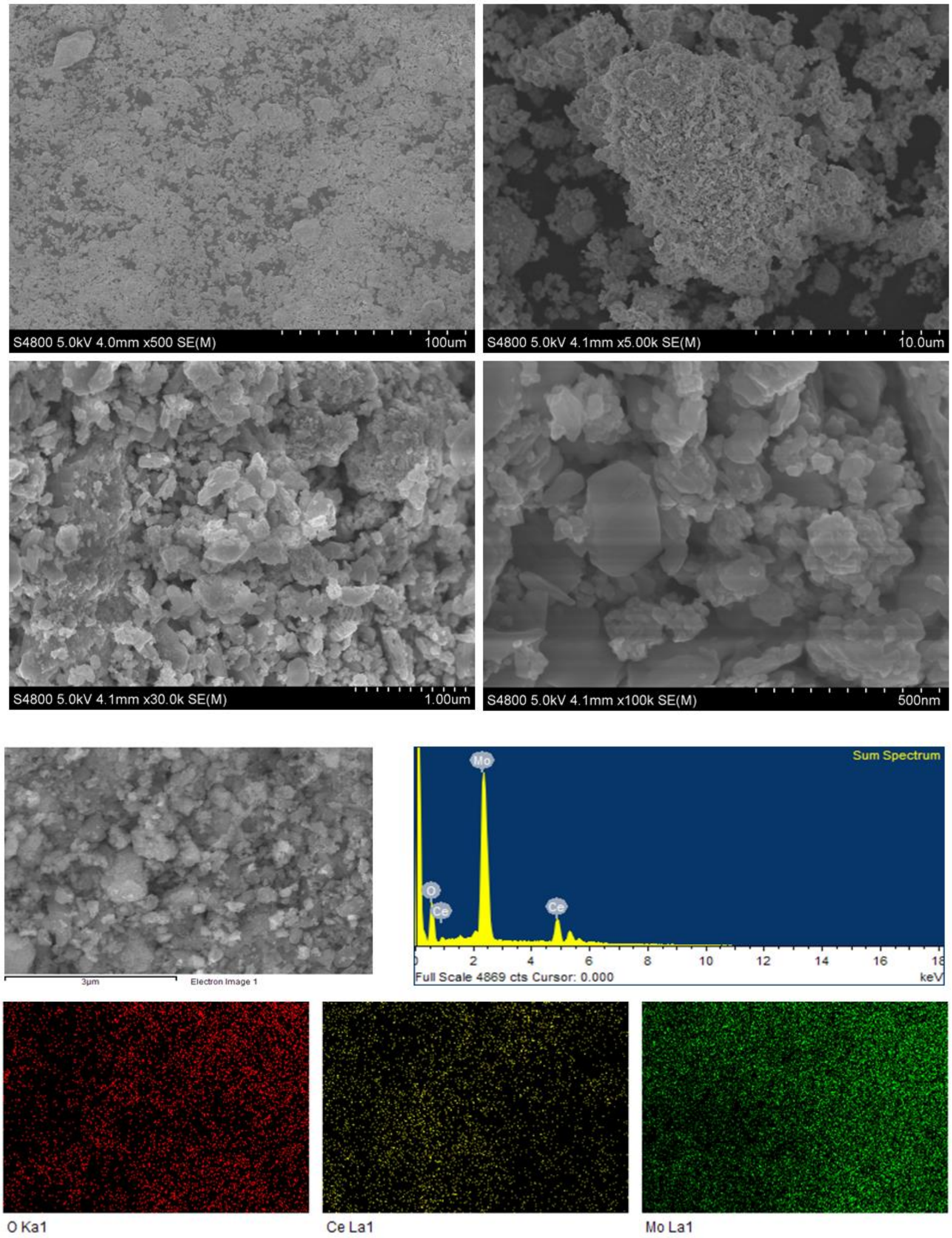

Fig. S10. SEM and SEM-EDS images of Mo-doped CeO_2.

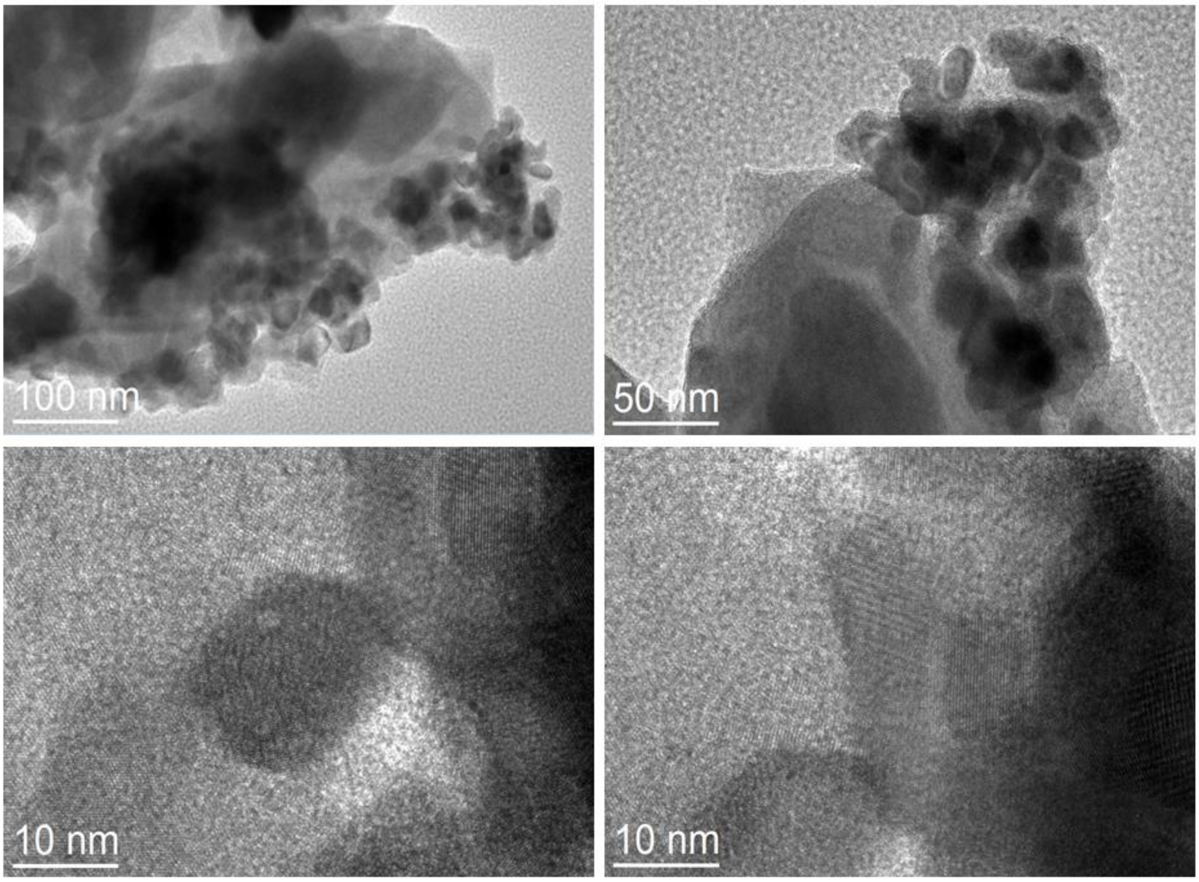

Fig. S11. TEM images of Mo-doped CeO_2.

6. Catalyst stability

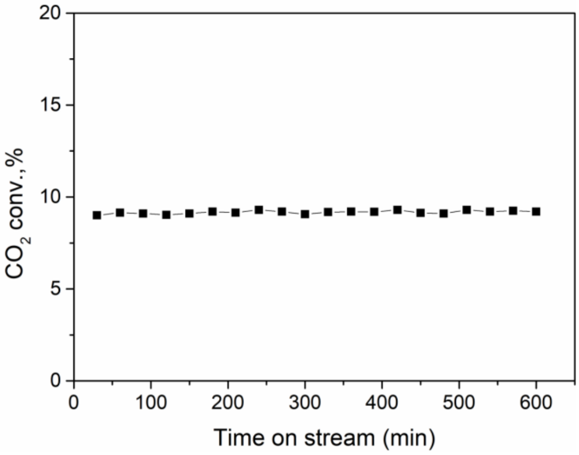

Fig. S12. CO_2 conversion as a function of time.

(CO_2 flow rate 40 ml/min, reaction temperature 400 °C, SEI 20 kJ/L, discharge power 13.5 W)

7. FTIR analysis

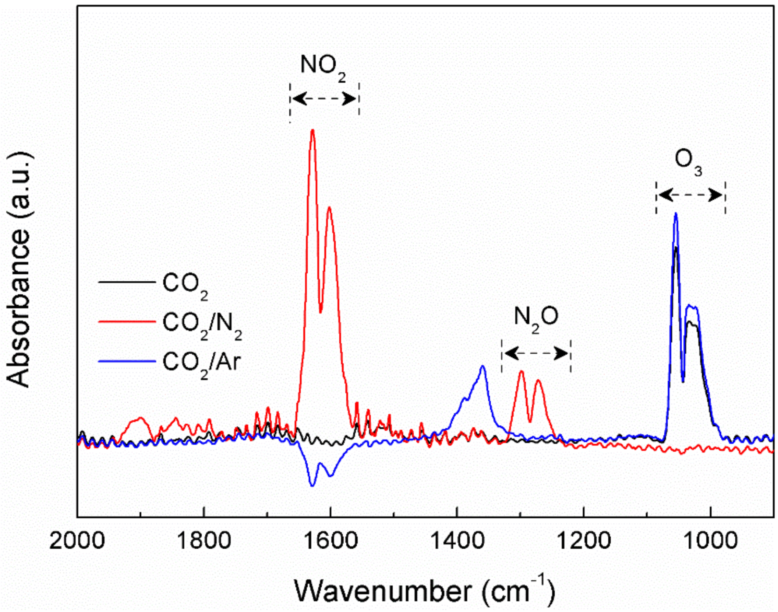

Fig. S13. FTIR spectra of by-products in the plasma-catalytic CO_2 splitting over Mo-doped CeO_2 with and without additive gas

8. Current signals of CO_2 DBD

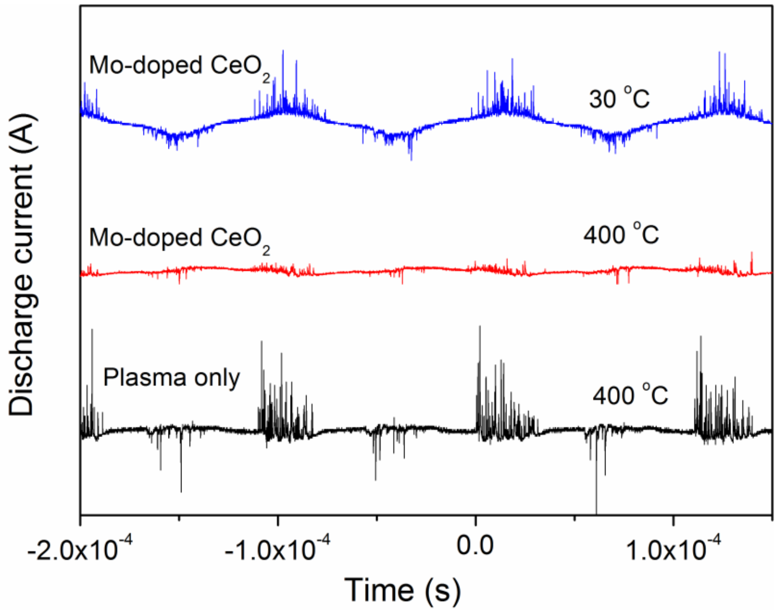

Fig. S14. Current signals of CO_2 DBD at different conditions.

(CO_2 flow rate 40 ml/min, SEI 20 kJ/L, discharge power 13.5 W)